PLOS ONE

RESEARCH ARTICLE

Lung aeration in experimental malaria-associated acute respiratory distress syndrome by SPECT/CT analysis

Thatyane de Castro Quirino[1☯], Luana dos Santos Ortolan[2¤‡], Michelle Klein Sercundes[1‡], Claudio Romero Farias Marinho[3], Walter Miguel Turato[1,4☯], Sabrina Epiphanio[1]*

1 Departamento de Análises Clínicas e Toxicológicas, Faculdade de Ciências Farmacêuticas, Universidade de São Paulo, São Paulo, Brasil, **2** Departamento de Imunologia, Instituto de Ciências Biomédicas, Universidade de São Paulo, São Paulo, Brasil, **3** Departamento de Parasitologia, Instituto de Ciências Biomédicas, Universidade de São Paulo, São Paulo, Brasil, **4** Centro de Radiofarmácia, Instituto de Pesquisas Energéticas e Nucleares, São Paulo, Brasil

☯ These authors contributed equally to this work.
¤ Current address: Seattle Children's Research Institute, Seattle, Washington, United States of America
‡ These authors also contributed equally to this work.
* sabrinae@usp.br

OPEN ACCESS

Citation: Quirino TdC, Ortolan LdS, Sercundes MK, Marinho CRF, Turato WM, Epiphanio S (2020) Lung aeration in experimental malaria-associated acute respiratory distress syndrome by SPECT/CT analysis. PLoS ONE 15(5): e0233864. https://doi.org/10.1371/journal.pone.0233864

Editor: Luzia Helena Carvalho, Instituto Rene Rachou, BRAZIL

Received: February 1, 2020

Accepted: May 13, 2020

Published: May 29, 2020

Data Availability Statement: All relevant data are within the manuscript and its Supporting Information files.

Funding: São Paulo Research Foundation (Fundação de Amparo à Pesquisa do Estado de São Paulo: FAPESP, Brazil), the Coordination of Improvement of Higher Level Personnel; (Coordenação de Aperfeiçoamento de Pessoal de Nível Superior: CAPES) and the National Council for Scientific and Technological Development (Conselho Nacional de Desenvolvimento Científico

Abstract

Malaria-associated acute respiratory distress syndrome (ARDS) is an inflammatory disease causing alveolar-pulmonary barrier lesion and increased vascular permeability characterized by severe hypoxemia. Computed tomography (CT), among other imaging techniques, allows the morphological and quantitative identification of lung lesions during ARDS. This study aims to identify the onset of malaria-associated ARDS development in an experimental model by imaging diagnosis. Our results demonstrated that ARDS-developing mice presented decreased gaseous exchange and pulmonary insufficiency, as shown by the SPECT/CT technique. The pulmonary aeration disturbance in ARDS-developing mice on the 5th day post infection was characterized by aerated tissues decrease and nonaerated tissue accumulation, demonstrating increased vascular permeability and pleural effusion. The SPECT/CT technique allowed the early diagnosis in the experimental model, as well as the identification of the pulmonary aeration. Notwithstanding, despite the fact that this study contributes to better understand lung lesions during malaria-associated ARDS, further imaging studies are needed.

Introduction

Malaria-associated acute respiratory distress syndrome (ARDS) is an acute inflammatory pulmonary lesion characterized by severe hypoxia [1,2], leading to vascular permeability increase [3,4], which causes pleural effusion and lung weight enlargement [5], and also reduces aerated lung tissue resulting in high mortality (30–40%) in intensive care units [6–8]. Seven species of Plasmodium, etiological malaria agents, have been identified as capable of infecting humans

e Tecnológico: CNPq, Brazil) supported this research. TCQ (CNPq 131431/2017-0), LSO (CAPES and FAPESP 2013/20718-3), MKS (CAPES/ PNPD), CRFM (FAPESP 2016/07030-3), SE (FAPESP 2017/05782-8) received fellowship grants. The funders had no role in study design, data collection and analysis, decision to publish, or preparation of the manuscript.

Competing interests: The authors have declared that no competing interests exist.

[9,10]. However, infections by *Plasmodium falciparum* and *Plasmodium vivax* showed 95% prevalence of malaria in the world [11]. In spite of the progress in its prophylaxis and treatment [12–14], malaria is still considered an important public health problem [15]. World Malaria Report published in 2019 showed an increase in malaria cases, stating 228 million human infections and 405 thousand deaths in 2018 [16].

Imaging procedures such as chest X-ray and computed tomography (CT) [17], gold standard techniques in ARDS identification [18], along with others, such as electrical impedance, positron emission tomography (PET) [19] and ultrasonography [20] are fundamental for diagnosis and analysis of lung function during ARDS development [21,22]. Through X-ray technique, it is possible to observe the opacity of bilateral diffuse infiltrate in humans lungs [23] and unilateral opacification in mice lungs [5]. On the other hand, pulmonary topographic analyzes during ARDS in mice demonstrate that the respiratory capacity has been decrease with normally aerated tissue reduction and increase nonaerated tissues. In addition, those lungs can be associated with atelectasis [24], ground-glass attenuation, consolidation in ARDS acute phase and reticulation attenuation with fibrosis in late phase [17].

The densitometry determines the lung compartments, according to X-ray attenuation values, and shows absence and presence of air inside the lungs, characterized by a voxel -700 Hounsfield Units (HU) which represents 70% gas and 30% tissue or water [25,26]. In addition, the lungs are characterized by hyperexpanded (-1000 to -900HU) compartments, normally aerated (-900 to -500HU), poorly aerated (-500 to -100HU) and nonaerated (0 to 100HU) [27–29]. Perfusion studies are critical to assess lung function and determine the blood flow available for gas exchange [30,31]. The main radionuclide used for single-photon emission computed tomography (SPECT) for diagnostic target is the metastable technetium 99 (^{99m}Tc) [32], a low energy gamma radiation emitter (140keV), which confers reduced cost and physical half- life of approximately six hours, making it possible to acquire high resolution scintigraphic images in gamma cameras [33,34]. The albumin macroaggregate (MAA) conjugated to ^{99m}Tc is a radiopharmaceutical with affinity for the lung and it is used in clinical diagnosis in nuclear medicine [35,36]. Furthermore, a better understanding of the pathogenesis and also the validation of new tools such as SPECT/CT studies are necessary for malaria-associated ARDS early diagnosis.

Materials and methods

Mice and ethics statement

DBA/2 male mice, 6–8 weeks old, specific pathogens free (SPF), were maintained in 12/12h light/dark cycle and acclimatized for 1 week before the experiments. The maximum of five mice per cage were housed in a standard polycarbonate cage with wood shavings bedding, an SPF animal house. We also attempted to reduce the stress of individual housing by environmental enrichment with small play tunnels. Mice had *ad libitum* access to food and water. The mice were initially imported from The Jackson Laboratory (USA) and the colonies were maintained in the Animal House of the Faculty of Pharmaceutical Sciences of the University of São Paulo (FCF/USP).

The experiments were performed according to the ethical guidelines established by the National Council for Control of Animal Experimentation (CONCEA: Conselho Nacional de Controle de Experimentação Animal) and Brazilian Federal Law nº 11.794 and approved by Animal Health Committee of the Biomedical Sciences Institute of the University of São Paulo (CEUA-ICB/USP, protocol number 05/2017). The ARRIVE guidelines recommendations are followed in this study.

Plasmodium berghei ANKA infection, parasitemia and euthanasia

Ten to twelve male DBA/2 mice per group were injected with 10^6 *P. berghei* ANKA (clone 1.49L)-infected red blood cells (iRBCs), kindly provided by the laboratory of Dra. Maria Mota from the institute of Molecular Medicine (IMM) in Portugal, by intraperitoneal route, as previously described [5,37]. Parasitemia was expressed as percentage of iRBCs and was determined by Giemsa staining. After infection, mice clinical signs were evaluated twice a day. Mortality was monitored from the 5th to 17th day post infection (dpi). The experimental time course to was reduced to 17 days after infection, compared with other experiments of our model previously published [5,37–39] to shorten any discomfort, pain or suffering that *Plasmodium berghei* infection may cause.

The euthanasia of DBA/2 mice was executed on the 17th dpi, using ketamine (150 mg/kg)/xylazine (15 mg/kg). Consciousness was checked by testing the pedal reflex, heartbeats, and breathing movements. In addition, the mice were humanely euthanized (end point) once they showed the following clinical signs: lethargy, hypothermia, and/or difficulty to breathe [measure in a whole-body plethysmography chamber (WBP, Buxco Electronics, Wilmington, North Carolina, USA)]. If these parameters were not properly registered, failing to achieve basal levels, it meant the mice were having severe breathing problems and consequently, euthanized.

Image protocol

The experiments were performed by using PET/SPECT/CT Albira 5.0 scanner system (Carestream Molecular Imaging, Woodbridge, CT, USA). *Plasmodium berghei* ANKA-infected (5th dpi, 7th dpi, 14th dpi) and healthy DBA/2 male mice were anesthetized intramuscularly or subcutaneously with Ketamine (100mg/kg) and Xilazine (10mg/kg). They were placed in prona position for images acquisition. Pulmonary perfusion was performed with 50–100μl of 258μCi of ^{99m}Tc-MAA (Pul-Tec, IPEN, São Paulo, Brazil) by intravenous route. The SPECT/CT acquisition was performed using single pinhole collimators in a 50 mm field view, being the energy and X-ray current characteristics 35 kVp and 400 μA, respectively. The simplified protocol of the methodology sequence for image acquisition is described in S1 Fig.

3D reconstruction of SPECT/CT images

Initial SPECT and CT data were reconstructed with Ordered-Subsets Expectation Maximization (OSEM) and Filtered Back Projection (FBP) algorithms by using Albira suite reconstruction and μPMOD version 5.0 (PMOD technologies, Zurich, Switzerland) softwares, in order to obtain images with spatial resolution of 1.8 mm and 0.125 mm, respectively. Mask and cropped tools were applied in the initial files so that lungs were segmented in different aeration threshold. A total of 1,000 projections/mice for CT and 60 projections/mice for SPECT were performed at 30 second/projection duration and approximately 1 hour and 20 min for total acquisition.

Quantitative analysis of SPECT/CT images

The SPECT and CT images were quantified using the μPMOD version 5.0 program (PMOD technologies, Zurich, Switzerland). Briefly, each CT image was segmented according to HU values. For each region of interest (ROI), in right and left lungs, 3D segmentation was performed, in which the voxels number was calculated, evaluating their respective mass and volume, using 25/25 HUs as the initial threshold [27,40]. In this study, we determined the pulmonary compartments as follows: hyperexpanded (-1000 HU to -900 HU), normally aerated (-900 HU to -500 HU), poorly aerated (-500 to -100 HU) and nonaerated (-100 to +100 HU). For pulmonary perfusion, ^{99m}Tc-MAA activity analysis was used and the images were

processed using the 3D Slicer version 4.8 (3DSlicer technologies, Harvard, USA) employing the Segment Editor to select the ROI and the threshold tool.

Respiratory parameters quantification

Mice respiratory parameters (respiratory rate, enhanced pause (Penh), inspiratory and expiratory time, ventilation volume and tidal volume) were collected and quantified using unrestrained whole-body plestimography chambers (Buxco Eletronics, Harvard, USA) and FinePointe software, as previously described [39] on the 5th and 7th dpi.

Statistical analysis

The quantitative variables were presented as mean ± standard deviation (SD), being their normality data verified by Kolmogorov or Shapiro-Wilk tests. Nonparametric data were compared using Mann-Whitney test (2 groups) or Kruskal-Wallis (3 groups) followed by Dunn's post-hoc test. In the nonparametric correlation analysis, the Spearman test (r) was used, followed by the linear regression test. The differences between the groups were considered significant when $p < 0.05$. All data were analyzed using GraphPad Prism 5.0 software.

Results

Malaria-associated acute respiratory distress syndrome characterization in a murine model

During plasmodium infections, survival, parasitemia and respiratory parameters (respiratory rate, Penh, inspiratory and expiratory time, ventilation volume and tidal volume) were analyzed in order to identify the mice developing ARDS or Hyperparasitemia (HP) (Fig 1). The ARDS-developing mice, which died between 7th and 12th dpi (Fig 1A), showed pulmonary edema and hemorrhage as previously reported [4,5]. On the other hand, HP-developing mice which died after 13th dpi, showed pale and grayish lungs due to malarial pigment accumulation and anemia, as related before [5]. The parasitemia showed no significant differences between ARDS-developing and HP-developing mice, on the 5th dpi, but it was higher in the former, on the 7th dpi ($p<0.05$) (Fig 1B). In addition, ARDS-developing mice, on the 7th dpi, showed decreased respiratory frequency (Fig 1C), increased enhanced pause (Fig 1D), diminished tidal volume (Fig 1E), reduced ventilation volume (Fig 1F), prolonged expiration time (Fig 1G), but did not show significant differences in inspiration time (Fig 1H) when compared to those non-infected or HP-developing mice.

Imaging diagnosis of experimental malaria-associated acute respiratory distress syndrome analyzed by computed tomography

The qualitative analysis of pulmonary aeration during experimental ARDS (Fig 2), demonstrated that ARDS-developing mice, on the 7th dpi, had a marked decrease in aeration extensive areas compatible with consolidation associated with diffuse opacification in all topographic cuts, when compared to HP-developing, ARDS-developing (on the 5th dpi) and non-infected mice, which had healthy lungs and intense aeration. HP-developing mice showed decreased aerated tissues and marked opacification, on the 7th dpi, when compared with the 5th dpi and with non-infected mice.

However, HP-developing mice showed increased aerated lung tissue, on the 14th dpi, when compared with the 7th dpi. The predominance of ground-glass opacification pulmonary lesions in ARDS-developing mice, on the 7th dpi, demonstrating alveolar collapse followed by a decrease in respiratory capacity was observed.

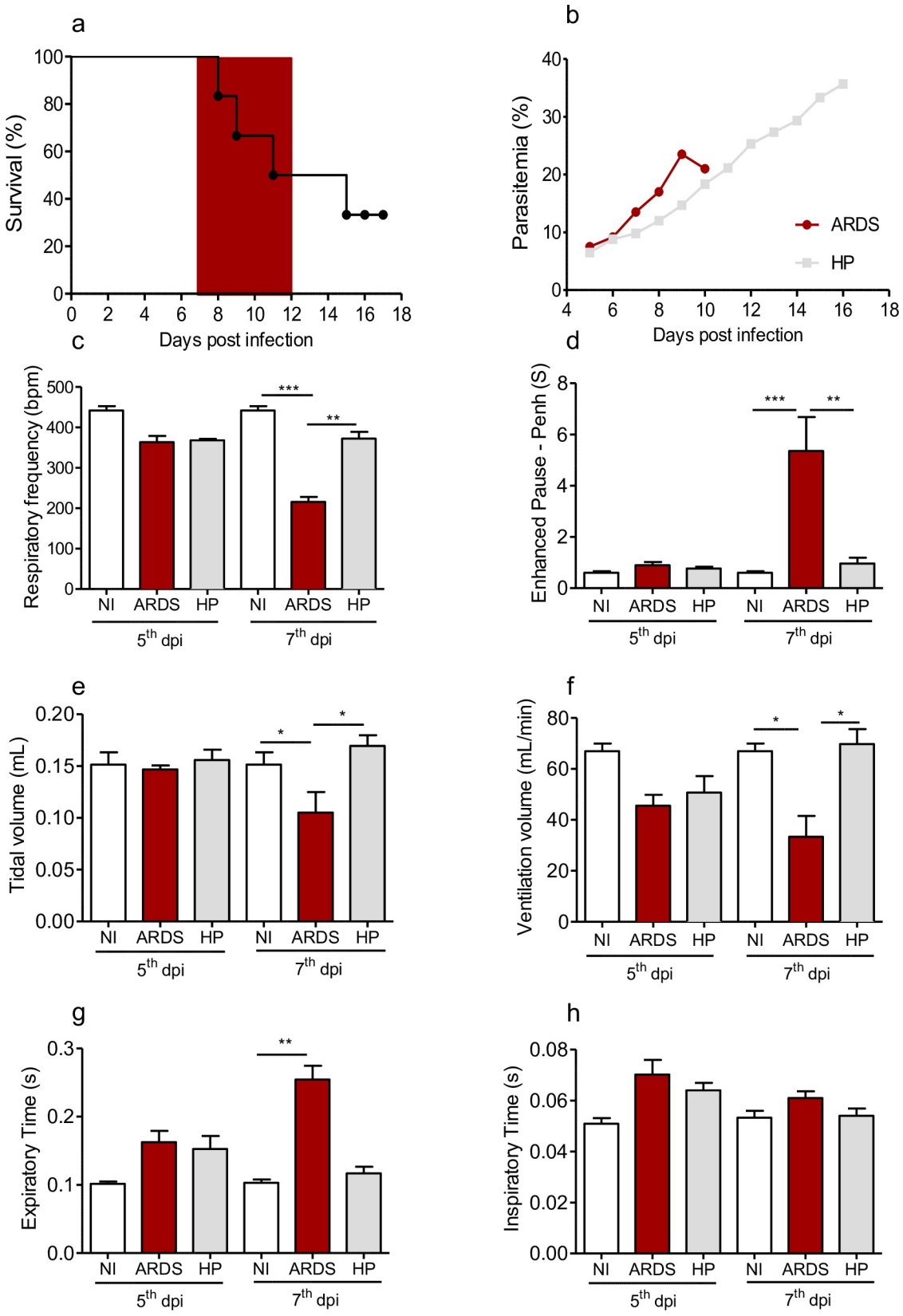
a
Survival (%)
Days post infection
b
Parasitemia (%)
ARDS
HP
Days post infection
c
Respiratory frequency (bpm)
d
Enhanced Pause - Penh (S)
e
Tidal volume (mL)
f
Ventilation volume (mL/min)
g
Expiratory Time (s)
h
Inspiratory Time (s)
NI
ARDS
HP
5th dpi
7th dpi

Fig 1. Evaluation of survival, parasitemia and respiratory parameters during malaria-associated ARDS in experimental model. (a) Survival curve, (b) parasitemia, (c) respiratory frequency, (d) enhanced pause (Penh), (e) tidal volume, (f) ventilation volume, (g) exhalation time and (h) inspiration time in *Plasmodium berghei*-infected DBA/2 mice on the 5th and 7th days post infection (dpi). The ARDS-developing mice died between 7th and 12th dpi, identified by gray band (a). Data presented as mean and standard error. Kruskal-Wallis Test, * $p < 0.01$, ** $p < 0.001$, ** $p < 0.0001$, n = 7–12 mice/ experiment. Representative figures from 2–3 independent experiments NI: Non-Infected mice, ARDS: Acute Respiratory Distress Syndrome, HP: Hyperparasitemia.

https://doi.org/10.1371/journal.pone.0233864.g001

Experimental malaria promotes lung aeration reduction analyzed by computed tomography

In the 3D reconstructions and quantification of the pulmonary aeration (Fig 3), we could observe small areas of hyperinflation in the coronal topographies of non-infected and *P. berghei* ANKA-infection mice promoted an evident reduction in hyperexpanded tissues in DBA/2 mice, when compared to those non-infected, during all days of analyzes. However, there was no significant difference between ARDS-developing and HP-developing, on the 5th and 7th dpi (Fig 3A and 3B).

Non-infected mice presented higher values of normally aerated tissue when compared to *P. berghei* ANKA-infected ones in all the analyzed days (Fig 3A and 3C). Nonetheless, ARDS-developing mice, on the 5th and 7th dpi, showed the lowest values of normally aerated, exhibiting pulmonary commitment (NI vs ARDS on the 5th dpi $p < 0.001$, NI vs ARDS on the 7th dpi $p < 0.001$). No significant differences were observed in pulmonary aeration between ARDS-developing and HP-developing mice on the 5th or 7th dpi ($p > 0.05$). Interestingly, ARDS-developing mice showed a decrease in aerated (hyperexpanded and normally aerated) tissues on the 5th dpi ($p < 0.01$), suggesting that the longitudinal evaluation may allow the detection of ARDS alterations earlier, once the aeration profile of HP-developing did not change on the 5th dpi when compared to those mice on the 7th dpi ($p > 0.05$). On the other hand, on the 14th dpi, the lungs of the HP-developing mice exhibited the most conserved areas, displaying pulmonary lesions reduction (Fig 3A and 3C).

Regarding poorly aerated tissues, HP-developing mice showed a significant decrease when compared to ARDS-developing, on the 5th dpi ($p > 0.01$), but, on the 7th dpi, ARDS-developing exhibited tissues decrease when compared to HP-developing and non-infected mice ($p > 0.001$). ARDS-developing mice, on the 5th and 7th dpi, did not demonstrate poorly aerated tissue differences when compared to those non-infected. Also, we observed an increase in poorly aerated tissues in HP-developing mice on the 14th dpi when compared to those on the 7th dpi. ($p > 0.01$) (Fig 3A and 3D).

Non-infected mice showed small areas of non-aerated tissues and, after infection, these regions increased on all analyzed days when compared to controls. ARDS-developing mice showed interesting results regarding nonaerated tissues, which increased when compared to all other mice. On the 7th dpi, ARDS-developing mice presented approximately 80% of non-aerated lung tissues, reaching 4-fold increase compared to non-infected ones, demonstrating increased pulmonary vascular permeability and, consequently, fluid accumulation (edema), hemorrhages and congestion areas. Finally, ARDS-developing mice, on the 5th dpi, presented 2-fold increase of those tissues when compared to the controls, allowing early identification of pulmonary collapse (Fig 3A and 3E).

Increased non-aerated lung tissue is related to respiratory capacity during experimental malaria-associated ARDS

On the 5th dpi, there was no correlation between respiratory parameters, as respiratory frequency, increased respiratory pause, inspiratory and expiratory time, ventilation volume and

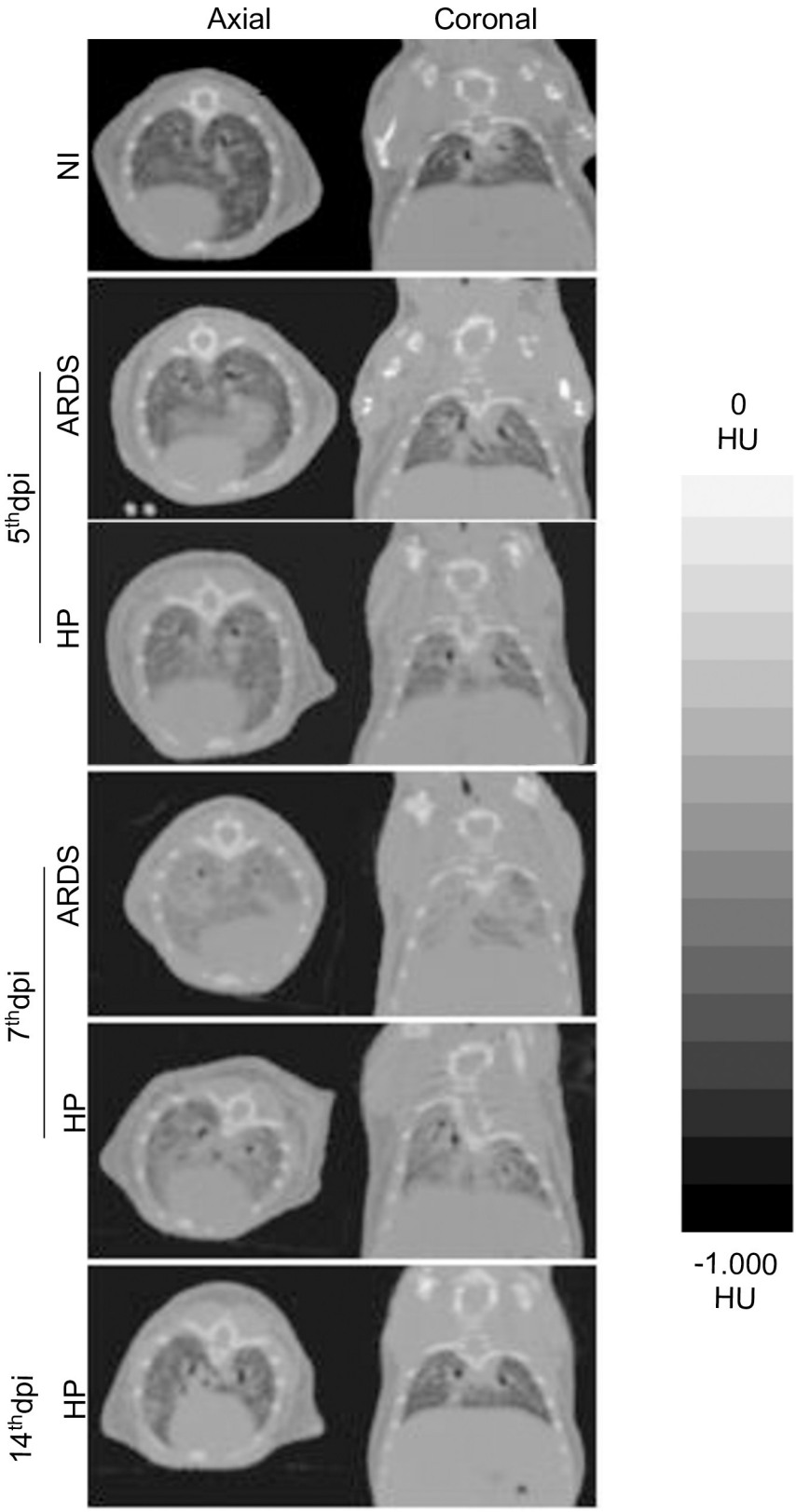

Fig 2. Morphological evaluation during the development malaria-associated ARDS by computed tomography. Representative topographic images of *P. berghei* ANKA-infected DBA/2 mice. The scale by Hounsfield Units 0 HU

(Water Density) to -1,000 HU (Air Density). Representative figures from 2–4 independent experiments, n = 7–14 animals/experiment. NI: Non-Infected mice, ARDS: Acute Respiratory Distress Syndrome, HP: Hyperparasitemia; dpi: days post infection.

https://doi.org/10.1371/journal.pone.0233864.g002

tidal volume, and CT data, because there weren't differences in these respiratory parameters between non-infected and infected mice. However, performing the linear regression on the 7th dpi, we observed a correlation between these respiratory parameters and an increase in non-aerated tissues (Fig 4). ARDS-developing mice presented a strong negative correlation between decrease of respiratory rate and increase of non-aerated tissue (R^2 0.88 $p<0.005$) (Fig 4A); negative correlation between the decrease of ventilation volume and increase in non-aerated tissues (R^2 0.89 $p <0.004$) (Fig 4B); negative correlation between the decrease of tidal volume and increase of non-aerated tissue (R^2 0.53 $p <0.01$) (Fig 4C); positive correlation between increased enhanced pause and non-aerated tissues (R^2 0.94 $p <0.001$) (Fig 4D) and between increased expiration time and non-aerated tissue (R^2 0.95 $p <0.001$) (Fig 4E); positive correlation between increased inspiratory time and increased atelectasis (R^2 0.87 $p <0.006$) (Fig 4F).

ARDS-developing mice analyzed by SPECT show decreased pulmonary perfusion

Pulmonary function was assessed, and our results showed a decrease of ^{99m}Tc-MAA activity during pulmonary perfusion assay in ARDS-developing mice on the 7th dpi (Fig 5A) in all topographic plans, when compared to non-infected and HP-developing mice. In addition, in ARDS-developing mice, we observed a different pattern of blood flow, characterized by marked reduction of perfusion in the left lung and absence of uniform radiopharmaceutical distribution, when compared to non-infected and HP-developing mice (Fig 5B), because these former mice showed no or lower inflammatory process, compared to ARDS-developing mice, demonstrating larger pulmonary distribution of the radiopharmaceutical.

Discussion

Considering the critical ability to study vital pulmonary processes as well as the understanding of ARDS development, we used a SPECT/CT methodology to measure the respiratory capacity in experimental malaria-associated ARDS using *Plasmodium berghei* ANKA-infected DBA/2 mice. The choice of murine model to this study, malaria-associated ARDS using *Plasmodium berghei* ANKA-infected DBA/2 mice, is due to its high reproducibility and effectiveness, showing also great similarity to ARDS patients [4,5]. Others models of experimental ARDS were reported using *P. berghei*-infected C57BL/6 mice [41,42]. However, it is not possible to previously predict which mice will develop ARDS or not, and sometimes, these mice could develop cerebral malaria [43–45].

This preclinical tool can support future investigations into the pathogenesis of ARDS, helping to fill the gap for clinical comprehension of the disease. Changes in respiratory parameters are crucial to identify lung injury in ARDS patients [46]. The reduced respiratory rate and increased pulmonary resistance, due to deficiency in pulmonary oxygenation, makes the ventilatory state monitoring fundamental to prevent the death of the patient [47].

The predictive criteria have been developed to identify the development of experimental malaria-associated ARDS before death, using parasitemia, breath frequency and enhanced pause (Penh), measured on the 7th dpi, recognizing the progress to ARDS or not (5). In this predictive model, it is not possible to identify the development of ARDS earlier, before 7th dpi, because on the 5th dpi there are no significant differences in these parameters, which is possible

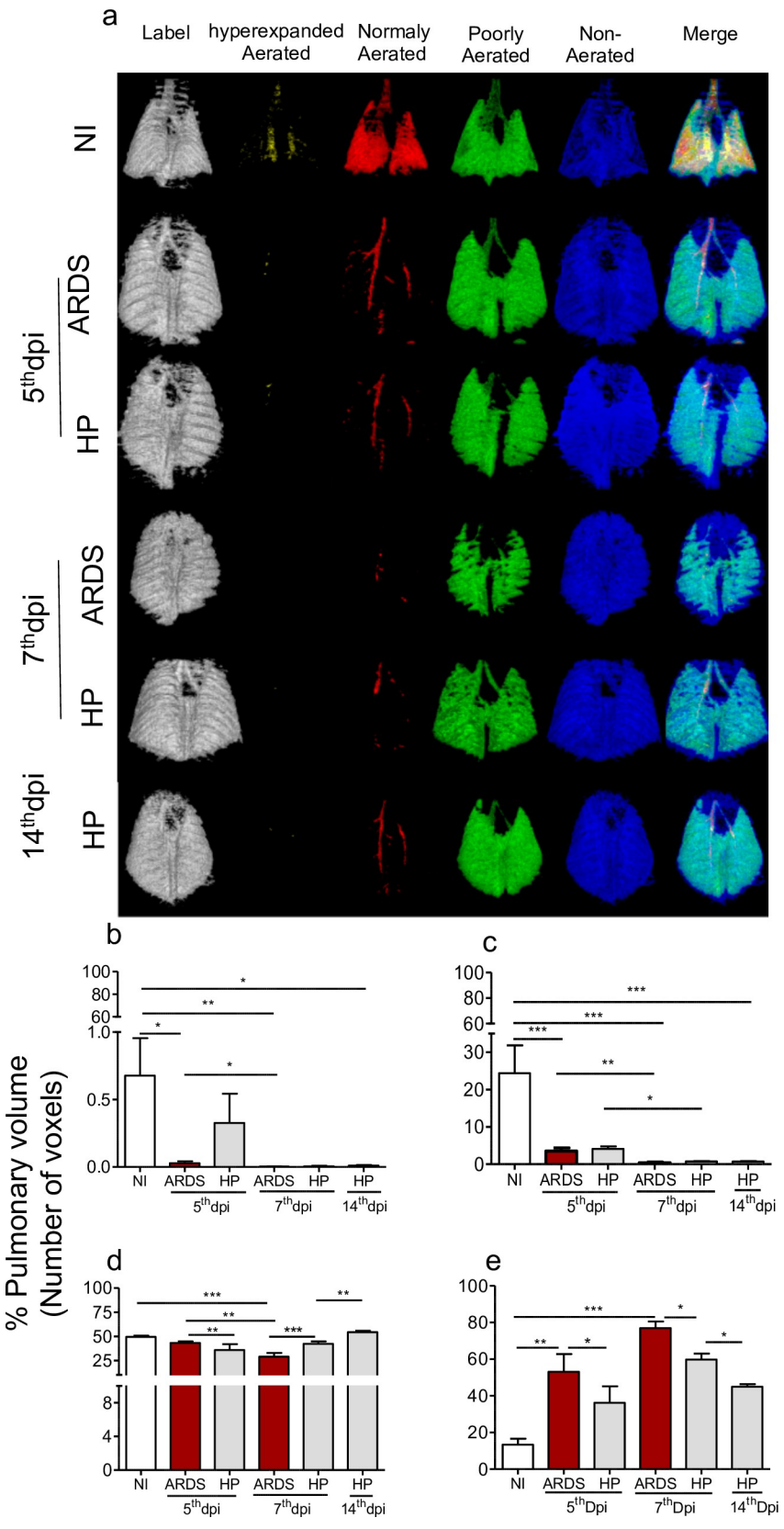
a
Label
hyperexpanded Aerated
Normaly Aerated
Poorly Aerated
Non-Aerated
Merge
NI
5thdpi
ARDS
HP
7thdpi
ARDS
HP
14thdpi
HP
b
c
% Pulmonary volume (Number of voxels)
d
e
NI
ARDS
HP
5thdpi
7thdpi
14thdpi
5thDpi
7thDpi
14thDpi

Fig 3. Malaria-associated ARDS decreases pulmonary aeration and promotes atelectasis as shown in computed tomography. (a) Coronary posterior plane 3D pulmonary segmentation; Gray: Label CT, Yellow: Hyperexpanded, Red: Normally Aerated, Green: Poorly Aerated, Blue: Non-Aerated, Overlap: Merge. (b-e) Quantification of pulmonary aeration by computed tomography in DBA/2 mice after 5th, 7th, and 14th days of *Plasmodium berghei* ANKA infection. (b) hyperexpanded aerated tissues; (c) Normally aerated tissues; (d) Poorly aerated tissues; (e) Non-aerated tissues; Representative images of 2 independent experiments, n = 8-12/experiment. Kruskal-Wallis. * $p < 0.05$, ** $p < 0.01$, ** $p < 0.001$. NI: Non-Infected, ARDS: Acute respiratory distress syndrome, HP: Hyperparasitemia, dpi: days post infection.

https://doi.org/10.1371/journal.pone.0233864.g003

now through SPECT/CT diagnosis. In addition, we reinforce here the results presented by Ortolan et al., regarding hemorrhages, pulmonary edema and hydrothorax and worse respiratory capacity [5]. On the other hand, ARDS-developing mice on the 7th dpi showed higher parasitemia compared to those HP-developing.

Tidal volume, which is correlated with pulmonary compliance and respiratory acidosis during the development of ARDS, is critical for monitoring patients and demonstrates inadequate pulmonary ventilation and the necessity of positive end-expiratory pressure (PEEP) adjustments to reduce the risk of death in 22% of patients in intensive therapy units [47–49]. Our results showed a reduction in tidal volume in ARDS-developing mice, corroborating the difficulty in breathing capacity.

ARDS patients present an increase in inspiratory pause [50] and inspiratory time [51], due to deficiency in pulmonary gas exchange, inducing barotrauma. Also, it is observed in these patients, extending expiration time, demonstrating the decreased ventilation and promoting pulmonary collapse [46]. Penh measurement during ARDS experimental model, which evaluates lung function noninvasively and ventilation volume, demonstrates the difficulty in gas exchange and pulmonary function failure [4,5,52–54], as observed in our results. However, as these measurements cannot be correlated with pulmonary resistance, ventilation mechanism studies are necessary [55].

Imaging techniques as well as chest radiography and computed tomography have been used to ARDS diagnosis [56] and also to malaria patients, allowing the identification of diffuse bilateral opacification and other lung lesions [6,57]. However, in our murine model, we observed the predominance of diffuse unilateral opacification [5] and in lipopolysaccharide model no predisposing lesions (apex or pulmonary base) were detected [18].

Morphological analysis of lung tissues are essential for ARDS diagnosis but it is necessary that two experienced radiologists confirm the lesions, which makes the quantitative analyzes fundamental to optimize processing time and promotes greater diagnostic accuracy [58,59]. The main lesions during ARDS, in the acute phase, are characterized by intense areas of ground-glass attenuation which demonstrates low aeration and consolidation, displaying pleural effusion and increased pulmonary permeability [18,60–62]. In the late phase, it is still possible to observe the reticulation attenuation demonstrating interlobular septal thickening, due to inflammatory cells and fibrosis accumulation [56,63,64]. Our results corroborate literature, since ARDS-developing mice demonstrated reduced pulmonary aeration and increased vascular permeability.

The decrease in pulmonary aeration ($> 40\%$) and the increase in vascular permeability are related to decreased compliance, due to a deficiency in the lung elastic properties during ARDS [26,65]. These findings are compatible with our results since the ARDS-developing mice present an increase in vascular permeability evidenced by pleural effusion reaching 1 ml of fluid in the thoracic cavity, which would complicate compliance. Our previous results showed increased pulmonary vascular permeability in malaria infection in DBA/2 model both *in vivo* and *in vitro* [4,5,38,39]. In addition, we observed that, after 14th dpi, an improvement in lung aeration when compared to that on the 7th dpi. Also, the baseline respiratory frequency

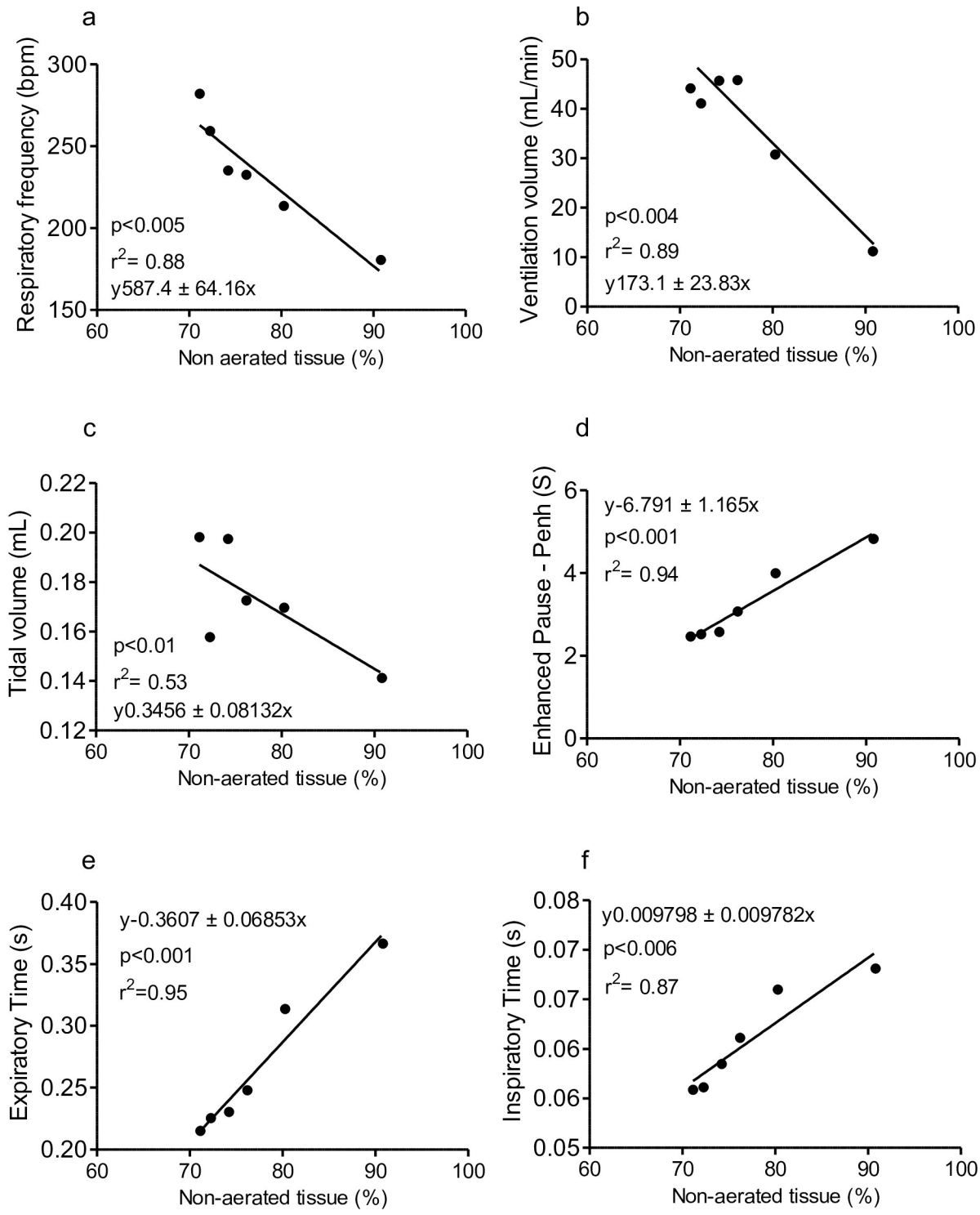

Fig 4. Correlation between non-aerated lung tissue by computed tomography with respiratory parameters during malaria-associated ARDS. (a) Strong negative correlation between decreased respiratory parameters with increased non-aerated CT tissue ($p < 0.005$). (b) Moderate negative correlation between volume per minute of ventilation with increased non-aerated CT tissue. (c) Moderate negative correlation between tidal volume with the increase of non-aerated CT tissue ($p < 0.01$. (d) Strong positive correlation between increased respiratory pause with the presence of non-aerated CT tissue ($p < 0.001$). (e) Strong positive correlation between expiration time with increased non-aerated CT tissue ($p < 0.001$). (f) Strong positive correlation between inspiratory time with increased non-aerated CT tissue ($p < 0.006$). Data presented as mean ± SD. Correlation: Linear Regression (R2) test, n = 6 mice.

https://doi.org/10.1371/journal.pone.0233864.g004

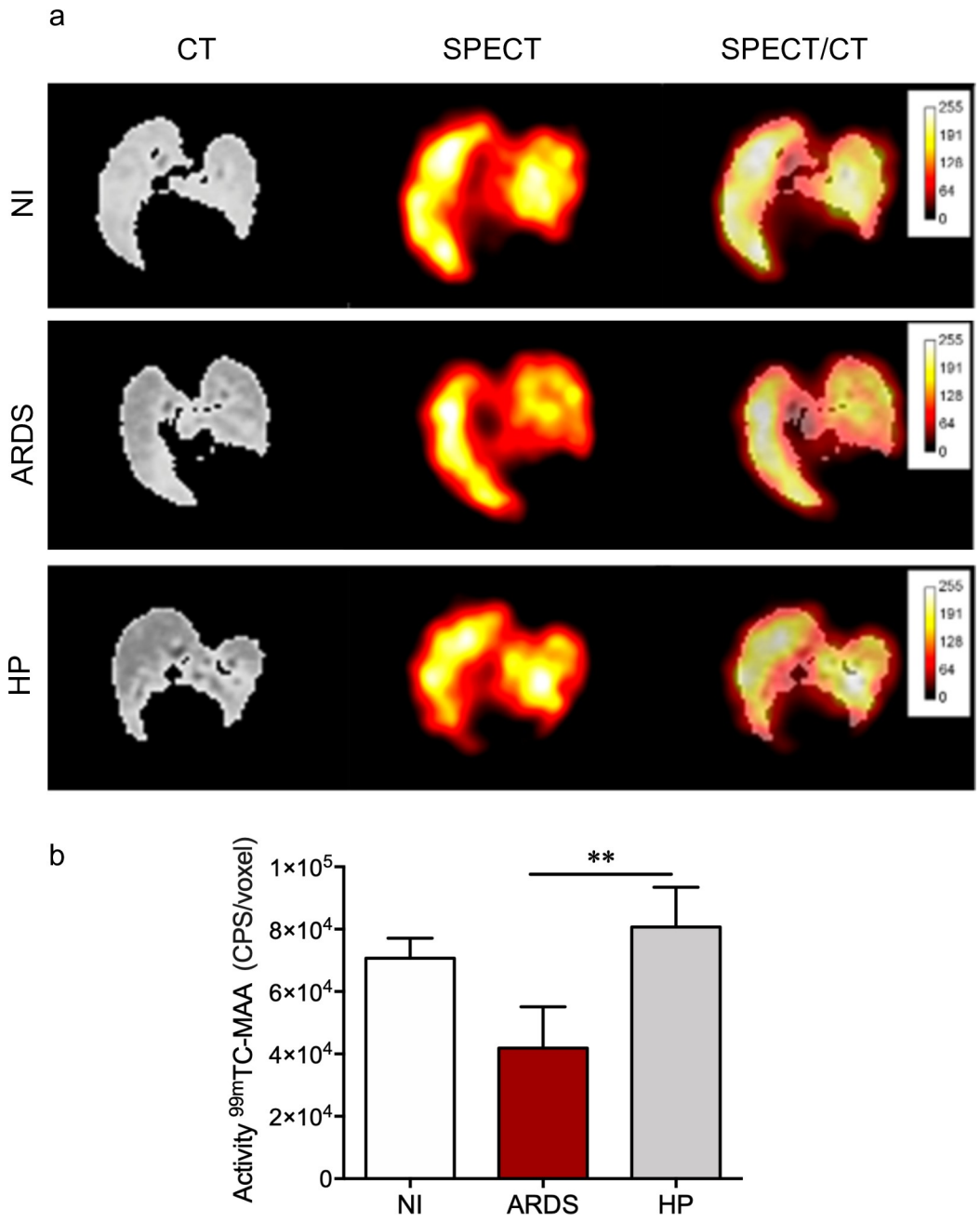

Fig 5. Malaria-associated ARDS promotes decreased ^{99m}Tc-MAA activity during pulmonary perfusion. (a) ARDS-developing mice presented absence of left lung perfusion in the coronal plane. (b) Reduced quantification of ^{99m}Tc-MAA activity in the lungs of ARDS-developing mice. Data represented as mean ± SD. One Way ANOVA, ** $p < 0.01$. Representative images of 2 isolated experiments, n = 7–10 mice/experiment. CPS/voxel: counts per second per voxel, NI: Noninfected mouse, ARDS: acute respiratory distress syndrome, HP: hyperpasitemia.

https://doi.org/10.1371/journal.pone.0233864.g005

and Penh in HP-developing mice, on the 21st dpi, returned to baseline, similar to that non-infected mice [5].

Chest computed tomography shows that 85% of the patients present bilateral lesions in the frontal segment of the left lung and only 5% of them do not exhibit these characteristics,

indicating a high sensitivity of this technique in ARDS lesions when compared to chest X-ray [66]. Alveolar-capillary increased permeability in these patients associated to decreased surfactant and lung inflammation induce atelectasis [65]. Pulmonary ventilation reduction is observed during ARDS, demonstrating pulmonary collapse, especially due to edema formation [67,68].

The CT is essential to prevent patients death in intensive care units. The reduction of ARDS patients mortality consists of not only hypoxia analysis, but also of PEEP, tidal volume and respiratory regulation assessment and adjustment which diminish lung collapse and overdistention, promoting protective mechanical ventilation [69,70].

The quantitative CT analysis shows that, during ARDS, deficit in gas exchange occurs with increased poorly aerated and nonaerated tissues and, decreased aerated tissues [71], in agreement with atelectasis, ground-glass opacification and consolidation attenuation areas [58], contributing to the reduction of pulmonary aeration [69]. High-resolution tomography is widely used in the measurement of pulmonary lesions and fibroproliferation in ARDS patients [72]. Segmentation of pulmonary aeration quantification during ARDS in both human and rodent models demonstrates to be an efficient tool for diagnosis, facilitating the data interpretation [24,71]. Recently, it has been described, in ARDS patients, a decrease in hyperinflated and normally aerated, reduction of poorly aerated and increase of nonaerated tissues, with values higher than 2-fold when compared to controls, demonstrating alveolar collapse and respiratory function failure [24]. Reduction in pulmonary aeration is observed in several human or animal ARDS models and proves to be a useful method for assessing atelectasis at the onset of lung injury [73–75].

The increase of nonaerated tissues is a milestone in the evaluation of pulmonary ventilation during ARDS [65], since these values can exceed 50 times those found in the voluntary controls, being CT an important tool to lung lesions identification. In addition, there is a decrease in hyperinflated and normally aerated tissues, especially on the right side of lungs [63,76]. Therefore, pulmonary aeration analysis during ARDS allows the identification of early diagnosis regarding to pulmonary oxygenation failures, which may prevent the high mortality of patients in the intensive care unit [77], including those malaria infected.

Measurement of pulmonary oxygenation is important to assess the severity of ARDS and is correlated with increased nonaerated tissues and atelectasis [73]. The degree of hypoxemia can be related to CT findings [71], in which low PaO_2 levels are linked to increased atelectasis areas and high shunt values [78]. In previous results, it was demonstrated, in our murine model, that hypoxemia was related to macroscopic and histological findings in ARDS-developing mice [4,5].

The respiratory mechanics, mainly perfusion, is essential to understand ARDS physiopathology [79]. During ARDS developing, the pulmonary perfusion is reduced in poorly aerated areas, which enables observation of radiopharmaceutical accumulation in the lesion, probably due to the increase of vascular permeability and higher blood bioavailability containing the radiopharmaceutical [60]. However, pulmonary alterations by CT are not always correlated with SPECT, as in lung cancer, in which there is marked decrease in aeration and intense areas of ground-glass, although the tissue analyzed by SPECT had been preserved [80].

Pulmonary perfusion in ARDS patients demonstrated a marked increase in the pulmonary base due to endothelial barrier dysfunction [77]. The perfusion location, important to measure oxygenation and radiopharmaceutical decrease, occurs in poorly aerated and it is distributed randomly in areas during ARDS [81]. The study of pulmonary perfusion and ventilation is essential during ARDS, detecting severe pulmonary insufficiency in patients [70]. Therefore, we believe these tools are very important to malaria-associated ARDS early diagnosis, enabling a more efficient therapeutic follow-up and reducing these patients mortality.

Conclusions

The application of the quantitative computed tomography technique allowed the early diagnosis in malaria-associated ARDS, concerning two methodologies for respiratory profile quantification, allowing a higher accuracy in the pulmonary oxygenation identification and also showing failures in the distribution of blood flow in ARDS-developing mice. However, the application of the SPECT/CT methodology in the early diagnosis of malaria-associated acute respiratory distress syndrome in humans could be impaired in malaria endemic areas due to the difficulty in accessing nuclear medicine equipment. Nonetheless, PET/CT methodology associated with magnetic resonance may be further used to identify the location of the inflammatory process and injuries during malaria-associated ARDS. On the other hand, for a better understanding of the pathophysiological mechanisms during ARDS, further studies should be developed.

Supporting information

S1 Fig. Summary protocol of SPECT/CT Image acquisition and processing process. Simplified representation of the methodology used in image acquisition and processing to provide the final perfusion data sets.
(TIF)

S1 Dataset.
(XLSX)

Acknowledgments

The authors thank Dr. Lorena Pozzo for supplying the ^{99m}Tc-MAA radiopharmaceuticals used in the study and Patricia Mendonça da Silva Amorim and Erika Paula Machado Peixoto for their technical assistance.

Author Contributions

Conceptualization: Thatyane de Castro Quirino, Luana dos Santos Ortolan, Claudio Romero Farias Marinho, Walter Miguel Turato, Sabrina Epiphanio.

Data curation: Thatyane de Castro Quirino.

Formal analysis: Thatyane de Castro Quirino, Michelle Klein Sercundes, Walter Miguel Turato, Sabrina Epiphanio.

Funding acquisition: Claudio Romero Farias Marinho, Sabrina Epiphanio.

Investigation: Luana dos Santos Ortolan, Walter Miguel Turato, Sabrina Epiphanio.

Methodology: Thatyane de Castro Quirino, Luana dos Santos Ortolan, Michelle Klein Sercundes, Walter Miguel Turato.

Project administration: Michelle Klein Sercundes, Sabrina Epiphanio.

Resources: Claudio Romero Farias Marinho, Sabrina Epiphanio.

Supervision: Luana dos Santos Ortolan, Claudio Romero Farias Marinho, Walter Miguel Turato, Sabrina Epiphanio.

Writing – original draft: Thatyane de Castro Quirino, Walter Miguel Turato, Sabrina Epiphanio.

Writing – review & editing: Thatyane de Castro Quirino, Luana dos Santos Ortolan, Michelle Klein Sercundes, Claudio Romero Farias Marinho, Walter Miguel Turato, Sabrina Epiphanio.

References

1. Rios F, Iscar T, Cardinal-Fernández P. What every intensivist should know about acute respiratory distress syndrome and diffuse alveolar damage. Rev Bras Ter Intensiva. 2017; 29: 354–363. https://doi.org/10.5935/0103-507X.20170044 PMID: 28977098
2. Ranieri VM, Rubenfeld GD, Thompson BT, Ferguson ND, Caldwell E, Fan E, et al. Acute respiratory distress syndrome: The Berlin definition. JAMA—J Am Med Assoc. 2012; 307: 2526–2533. https://doi.org/10.1001/jama.2012.5669 PMID: 22797452
3. Fanelli V, Vlachou A, Ghannadian S, Simonetti U, Slutsky AS, Zhang H. Acute respiratory distress syndrome: New definition, current and future therapeutic options. J Thorac Dis. 2013; 5: 326–334. https://doi.org/10.3978/j.issn.2072-1439.2013.04.05 PMID: 23825769
4. Epiphanio S, Campos MG, Pamplona A, Carapau D, Pena AC, Ataíde R, et al. VEGF promotes malaria-associated acute lung injury in Mice. PLoS Pathog. 2010; 6: 1–10. https://doi.org/10.1371/journal.ppat.1000916 PMID: 20502682
5. Ortolan LS, Sercundes MK, Barboza R, Debone D, Murillo O, Hagen SCF, et al. Predictive Criteria to Study the Pathogenesis of Malaria-Associated ALI/ARDS in Mice. Mediators Inflamm. 2014; 2014. https://doi.org/10.1155/2014/872464 PMID: 25276057
6. Elzein F, Mohammed N, Ali N, Bahloul A, Albadani A, Alsherbeeni N. Pulmonary manifestation of Plasmodium falciparum malaria: Case reports and review of the literature. Respir Med Case Reports. 2017; 22: 83–86. https://doi.org/10.1016/j.rmcr.2017.06.014 PMID: 28702342
7. AMATO M, ISOLA A, VIEIRA S, ROTMAN V, MOOCK M, JOSE A, et al. III Consenso Brasileiro de Ventilação Mecânica. J Bras Pneumol. 2007; 33: 128–136. https://doi.org/10.1590/S0004-27301999000400002
8. Ochiai R. Mechanical ventilation of acute respiratory distress syndrome. J Intensive Care. 2015; 3: 1–9. https://doi.org/10.1186/s40560-015-0091-6 PMID: 26045965
9. Brasil P, Zalis MG, de Pina-Costa A, Siqueira AM, Júnior CB, Silva S, et al. Outbreak of human malaria caused by Plasmodium simium in the Atlantic Forest in Rio de Janeiro: A molecular epidemiological investigation. Lancet Glob Heal. 2017. https://doi.org/10.1016/S2214-109X(17)30333-9
10. Calderaro A, Piccolo G, Gorrini C, Rossi S, Montecchini S, Dell'Anna ML, et al. Accurate identification of the six human Plasmodium spp. causing imported malaria, including Plasmodium ovale wallikeri and Plasmodium knowlesi. Malar J. 2013; 12: 1–6. https://doi.org/10.1186/1475-2875-12-321 PMID: 24034175
11. Loya DE, Liu W, Li Y, Learn GH, Plenderleithc LJ, Sundararaman SA, et al. HHS Public Access. 2017; 78: 401–411. https://doi.org/10.1002/ana.24447.Olfactory
12. Andrade JG. Terapêutica e profilaxia da malária. Revisão. Rev patol trop. 1994; 23: 181–190.
13. França TCC, Dos Santos MG, Figueroa-Villar JD. Malária: Aspectos históricos e quimioterapia. Quim Nova. 2008; 31: 1271–1278. https://doi.org/10.1590/S0100-40422008000500060
14. Tauil PL. Perspectivas de controle de doenças transmitidas por vetores no Brasil. Rev Soc Bras Med Trop. 2006; 39: 275–277. https://doi.org/10.1590/S0037-86822006000300010 PMID: 16906253
15. Siqueira-batista R, Vitorino R, Freitas RDB, Alberto L, Goreti M, Oliveira DA, et al. Malária por Plasmodium falciparum: estudos proteômicos. 2012; 24: 394–400. https://doi.org/10.1590/S0103-507X2012000400017 PMID: 23917939
16. World malaria report. World Malaria Report. Colombia. 2019.
17. Sheard S, Rao P, Devaraj A. Imaging of Acute Respiratory Distress Syndrome. Respir Care. 2012; 57: 607–612. https://doi.org/10.4187/respcare.01731 PMID: 22472500
18. Ma H, Huang D, Guo L, Chen Q, Zhong W, Geng Q, et al. Strong correlation between lung ultrasound and chest computerized tomography imaging for the detection of acute lung injury/acute respiratory distress syndrome in rats. J Thorac Dis. 2016; 8: 1443–1448. https://doi.org/10.21037/JTD.2016.05.15 PMID: 27499930
19. Bellani G, Mauri T, Pesenti A. Imaging in acute lung injury and acute respiratory distress syndrome. Curr Opin Crit Care. 2012; 18: 29–34. https://doi.org/10.1097/MCC.0b013e32834eb47d PMID: 22143052

20. Bello G, Blanco P. Lung Ultrasonography for Assessing Lung Aeration in Acute Respiratory Distress Syndrome A Narrative Review. J Ultrasound Med. 2018. https://doi.org/10.1002/jum.14671 PMID: 29732586

21. Worsley DF, Alavi A. Radionuclide Imaging of Acute Pulmonary Embolism. Semin Nucl Med. 2003; 33: 259–278. https://doi.org/10.1016/S0001-2998(03)00031-X

22. Jacene HA, Cohade C, Wahl RL. F-18 FDG PET/CT in acute respiratory distress syndrome: a case report. Clin Nucl Med. 2004; 29: 786–788. doi: 00003072-200412000-00002 [pii] PMID: 15545878

23. Rotta AT, Piva JP, Andreolio C, De Carvalho WB, Garcia PCR. Progress and perspectives in pediatric acute respiratory distress syndrome. Rev Bras Ter Intensiva. 2015; 27: 266–273. https://doi.org/10.5935/0103-507X.20150035 PMID: 26331971

24. Karmrodt J, Bletz C, Yuan S, David M, Heussel CP, Markstaller K. Quantification of atelectatic lung volumes in two different porcine models of ARDS. Br J Anaesth. 2006; 97: 883–895. https://doi.org/10.1093/bja/ael275 PMID: 17046849

25. Irion KL, Hochhegger B, Marchiori E, Porto NDS, Baldisserotto SDV, Santana PR. Chest X-ray and computed tomography in the evaluation of pulmonary emphysema | Radiograma de tórax e tomografia computadorizada na avaliação do enfisema pulmonar. J Bras Pneumol. 2007; 33: 720–732. https://doi.org/10.1590/S1806-37132007000600017 PMID: 18200374

26. Hochhegger B, Marchiori E, Irion KL, Oliveira H, Resumo A, Hochhegger Rua João Alfredo B. Accuracy of measurement of pulmonary emphysema with computed tomography: relevant points* Acurácia da mensuração do enfisema pulmonar na tomografia computadorizada: pontos importantes. Jul/Ago. 2010; 43: 260–265. https://doi.org/10.1590/S0100-39842010000400011

27. Gattinoni L, Caironi P, Pelosi P, Goodman LR. What has computed tomography taught us about the acute respiratory distress syndrome? Am J Respir Crit Care Med. 2001; 164: 1701–1711. https://doi.org/10.1164/rccm2103121

28. Gattinoni L MD, Presenti AM, Torresin AP, Baglioni SM, Rivolta MM, Rossi FM, et al. Adult respiratory distress syndrome profiles by computed tom. .: Journal of Thoracic Imaging. Journal of Thoracic Imaging. 1986. Available: http://journals.lww.com/thoracicimaging/Abstract/1986/07000/Adult_respiratory_distress_syndrome_profiles_by.5.aspx

29. Gattinoni L, Pelosi P, Pesenti A, Brazzi L, Vitale G, Moretto A, et al. CT scan in ARDS: Clinical and physiopathological insights. Acta Anaesthesiol Scand. 1991; 35: 87–96. https://doi.org/10.1111/j.1399-6576.1991.tb03404.x PMID: 1927233

30. Bajc M, Jonson B. Ventilation/Perfusion SPECT for Diagnosis of Pulmonary Embolism and Other Diseases. Int J Mol Imaging. 2011; 2011: 1–7. https://doi.org/10.1155/2011/682949 PMID: 21490731

31. Jobse BN, Rhem RG, Wang IQ, Counter WB, Stampfli MR, Labiris NR. Detection of Lung Dysfunction Using Ventilation and Perfusion SPECT in a Mouse Model of Chronic Cigarette Smoke Exposure. J Nucl Med. 2013; 54: 616–623. https://doi.org/10.2967/jnumed.112.111419 PMID: 23397007

32. Schwochau K. Technetium Radiopharmaceuticals—Fundamentals, Synthesis, Structure, and Development. Angew Chemie Int Ed English. 1994; 33: 2258–2267. https://doi.org/10.1002/anie.199422581

33. Khalil MM, Tremoleda JL, Bayomy TB, Gsell W. Molecular SPECT Imaging: An Overview. Int J Mol Imaging. 2011; 2011: 1–15. https://doi.org/10.1155/2011/796025 PMID: 21603240

34. Conway J. Lung imaging—Two dimensional gamma scintigraphy, SPECT, CT and PET. Adv Drug Deliv Rev. 2012; 64: 357–368. https://doi.org/10.1016/j.addr.2012.01.013 PMID: 22310158

35. Kniess T, Laube M, Wuest F, Pietzsch J. Technetium-99m based Small Molecule Radiopharmaceuticals and Radiotracers Targeting Inflammation and Infection. Dalt Trans. 2017. https://doi.org/10.1039/C7DT01735A PMID: 28829079

36. Akbar MU, Ahmad MR, Shaheen A, Mushtaq S. A review on evaluation of technetium-99m labeled radiopharmaceuticals. J Radioanal Nucl Chem. 2016; 310: 477–493. https://doi.org/10.1007/s10967-016-5019-7

37. Sercundes MK, Ortolan LS, Debone D, Soeiro-Pereira P V., Gomes E, Aitken EH, et al. Targeting Neutrophils to Prevent Malaria-Associated Acute Lung Injury/Acute Respiratory Distress Syndrome in Mice. PLoS Pathog. 2016; 12: 1–24. https://doi.org/10.1371/journal.ppat.1006054 PMID: 27926944

38. Pereira MLM, Ortolan LS, Sercundes MK, Debone D, Murillo O, Lima FA, et al. Association of Heme Oxygenase 1 with Lung Protection in Malaria-Associated ALI/ARDS. Mediators Inflamm. 2016; 2016. https://doi.org/10.1155/2016/4158698 PMID: 27974865

39. Ortolan L dos S, Sercundes MK, Moura GC, Quirino T de C, Debone D, Costa D de S, et al. Endothelial Protein C Receptor Could Contribute to Experimental Malaria- Associated Acute Respiratory Distress Syndrome. J Immunol Res. 2019; 2019: 18. https://doi.org/10.1155/2019/3105817

40. Hounsfield G.N. Computerized transverse axial scanning(tomography):Part I description of system. Br J Radiol. 1973; 46: 1016–1022. https://doi.org/10.1259/0007-1285-46-552-1016 PMID: 4757352

41. Van Den Steen PE, Geurts N, Deroost K, Van Aelst I, Verhenne S, Heremans H, et al. Immunopathology and dexamethasone therapy in a new model for malaria-associated acute respiratory distress syndrome. Am J Respir Crit Care Med. 2010; 181: 957–968. https://doi.org/10.1164/rccm.200905-0786OC PMID: 20093644

42. Souza MC, Silva JD, Pádua TA, Capelozzi VL, Rocco PRM, Henriques M das G. Early and late acute lung injury and their association with distal organ damage in murine malaria. Respir Physiol Neurobiol. 2013; 186: 65–72. https://doi.org/10.1016/j.resp.2012.12.008 PMID: 23328346

43. Ghazanfari N, Mueller SN, Heath WR. Cerebral malaria in mouse and man. Front Immunol. 2018;9. https://doi.org/10.3389/fimmu.2018.02016 PMID: 30250468

44. Ong PK, Melchior B, Martins YC, Hofer A, Orjuela-Sánchez P, Cabrales P, et al. Nitric Oxide Synthase Dysfunction Contributes to Impaired Cerebroarteriolar Reactivity in Experimental Cerebral Malaria. PLoS Pathog. 2013; 9. https://doi.org/10.1371/journal.ppat.1003444 PMID: 23818850

45. Pamplona A, Ferreira A, Balla J, Jeney V, Balla G, Epiphanio S, et al. Heme oxygenase-1 and carbon monoxide suppress the pathogenesis of experimental cerebral malaria. Nat Med. 2007; 13: 703–710. https://doi.org/10.1038/nm1586 PMID: 17496899

46. Sahetya SK, Goligher EC, Brower RG. Setting positive end-expiratory pressure in acute respiratory distress syndrome. Am J Respir Crit Care Med. 2017; 195: 1429–1438. https://doi.org/10.1164/rccm.201610-2035CI PMID: 28146639

47. Chen IC, Kuo J, Ko WJ, Shih HC, Kuo CD. Increased flow resistance and decreased flow rate in patients with acute respiratory distress syndrome: The role of autonomic nervous modulation. J Chinese Med Assoc. 2016; 79: 17–24. https://doi.org/10.1016/j.jcma.2015.10.001 PMID: 26589196

48. Patroniti N, Pesenti A. Low tidal volume, high respiratory rate and auto-PEEP: The importance of the basics. Crit Care. 2003; 7: 105–106. https://doi.org/10.1186/cc1883 PMID: 12720551

49. Guerrero T, Castillo R, Noyola-Martinez J, Torres M, Zhou X, Guerra R, et al. Reduction of pulmonary compliance found with high-resolution computed tomography in irradiated mice. Int J Radiat Oncol Biol Phys. 2007; 67: 879–887. https://doi.org/10.1016/j.ijrobp.2006.10.037 PMID: 17293238

50. Aguirre-Bermeo H, Morán I, Bottiroli M, Italiano S, Parrilla FJ, Plazolles E, et al. End-inspiratory pause prolongation in acute respiratory distress syndrome patients: effects on gas exchange and mechanics. Ann Intensive Care. 2016; 6. https://doi.org/10.1186/s13613-016-0183-z PMID: 27558174

51. Mercat A, Diehl JL, Michard F, Anguel N, Teboul JL, Labrousse J, et al. Extending inspiratory time in acute respiratory distress syndrome. Crit Care Med. 2001; 29: 40–44. https://doi.org/10.1097/00003246-200101000-00011 PMID: 11176158

52. Bates J, Lai-fook S, Pare P, Pride N. Correspondence The Use and Misuse of Penh in Animal Models of Lung Disease. 2002.

53. Aeffner F, Bolon B, Davis IC. Mouse models of acute respiratory distress syndrome. Toxicol Pathol. 2015; 43: 1074–1092. https://doi.org/10.1177/0192623315598399 PMID: 26296628

54. Verheijden KAT, Henricks PAJ, Redegeld FA, Garssen J, Folkerts G. Measurement of airway function using invasive and non-invasive methods in mild and severe models for allergic airway inflammation in mice. Front Pharmacol. 2014; 5 AUG: 1–9. https://doi.org/10.3389/fphar.2014.00190 PMID: 25161620

55. Lundblad LKA, Irvin CG, Hantos Z, Sly P, Mitzner W, Bates JHT. Penh is not a measure of airway resistance! [1]. Eur Respir J. 2007; 30: 805. https://doi.org/10.1183/09031936.00091307 PMID: 17906089

56. Zompatori M, Ciccarese F, Fasano L. Overview of current lung imaging in acute respiratory distress syndrome. Eur Respir Rev. 2014; 23: 519–530. https://doi.org/10.1183/09059180.00001314 PMID: 25445951

57. Saleri N, Gulletta M, Matteelli A, Caligaris S, Tomasoni LR, Antonini B, et al. Acute respiratory distress syndrome in Plasmodium vivax malaria in traveler returning from Venezuela. J Travel Med. 2006; 13: 112–113. https://doi.org/10.1111/j.1708-8305.2006.00024.x PMID: 16553597

58. Vergani G, Cressoni M, Crimella F, L'Acqua C, Sisillo E, Gurgitano M, et al. A Morphological and Quantitative Analysis of Lung CT Scan in Patients With Acute Respiratory Distress Syndrome and in Cardiogenic Pulmonary Edema. J Intensive Care Med. 2017. https://doi.org/10.1177/0885066617743477 PMID: 29161936

59. Sun X, Zhang H, Duan H. 3D Computerized Segmentation of Lung Volume With Computed Tomography. Acad Radiol. 2006; 13: 670–677. https://doi.org/10.1016/j.acra.2006.02.039 PMID: 16679268

60. Chiumello D, Froio S, Bouhemad B, Camporota L, Coppola S. Clinical review: Lung imaging in acute respiratory distress syndrome patients—an update. Crit Care. 2013; 17: 243. https://doi.org/10.1186/cc13114 PMID: 24238477

61. Pesenti A, Tagliabue P, Patroniti N, Fumagalli R. Computerised tomography scan imaging in acute respiratory distress syndrome. Intensive Care Med. 2001; 27: 631–639. https://doi.org/10.1007/s001340100877 PMID: 11398688

62. Simon M, Braune S, Laqmani A, Metschke M, Berliner C, Kalsow M, et al. Value of Computed Tomography of the Chest in Subjects With ARDS: A Retrospective Observational Study. Respir Care. 2016; 61: 316–323. https://doi.org/10.4187/respcare.04308 PMID: 26647453

63. Markstaller K, Eberle B, Kauczor HU, Scholz A, Bink A, Thelen M, et al. Temporal dynamics of lung aeration determined by dynamic CT in a porcine model of ARDS. Br J Anaesth. 2001; 87: 459–468. https://doi.org/10.1093/bja/87.3.459 PMID: 11517132

64. De Matos GFJ, Barbas CS V. Importance of computed tomography scans of the chest in the evaluation of patients with acute respiratory distress syndrome. Pulmão RJ. 2011; 20: 13–17. Available: http://www.sopterj.com.br/profissionais/_revista/2011/n_03/04.pdf

65. Rouby J-J, Puybasset L, Nieszkowska A, Lu Q. Acute respiratory distress syndrome: Lessons from computed tomography of the whole lung. Crit Care Med. 2003; 31: S285–S295. https://doi.org/10.1097/01.CCM.0000057905.74813.BC PMID: 12682454

66. Negrin LL, Prosch H, Kettner S, Halat G, Heinz T, Hajdu S. The clinical benefit of a follow-up thoracic computed tomography scan regarding parenchymal lung injury and acute respiratory distress syndrome in polytraumatized patients. J Crit Care. 2017; 37: 211–218. https://doi.org/10.1016/j.jcrc.2016.10.003 PMID: 27969573

67. Reske AW, Rau A, Reske AP, Koziol M, Gottwald B, Alef M, et al. Extrapolation in the analysis of lung aeration by computed tomography: A validation study. Crit Care. 2011; 15: R279. https://doi.org/10.1186/cc10563 PMID: 22112625

68. Atul Malhotra M. Low-Tidal-Volume Ventilation in the Acute Respiratory Distress Syndrome. 2007; 11: 1113–1120. https://doi.org/10.1016/j.pmrj.2014.02.014.Lumbar

69. Bachmann MC, Morais C, Bugedo G, Bruhn A, Morales A, Borges JB, et al. Electrical impedance tomography in acute respiratory distress syndrome. Crit Care. 2018; 22: 1–11. https://doi.org/10.1186/s13054-018-2195-6 PMID: 30360753

70. Christmann Wawrzeniak I, Regina S, Vieira R, Almeida Victorino J. Weaning from Mechanical Ventilation in ARDS: Aspects to Think about for Better Understanding, Evaluation, and Management. 2018; 2018. https://doi.org/10.1155/2018/5423639 PMID: 30402484

71. Klapsing P, Herrmann P, Quintel M, Moerer O. Automatic quantitative computed tomography segmentation and analysis of aerated lung volumes in acute respiratory distress syndrome—A comparative diagnostic study. J Crit Care. 2017; 42: 184–191. https://doi.org/10.1016/j.jcrc.2016.11.001 PMID: 28759880

72. Anan K, Ichikado K, Ishihara T, Shintani A, Kawamura K, Suga M, et al. A Scoring System with High-Resolution Computed Tomography to Predict Drug-Associated Acute Respiratory Distress Syndrome: Development and Internal Validation. Sci Rep. 2019; 9: 1–9. https://doi.org/10.1038/s41598-019-45063-9 PMID: 31197186

73. Gattinoni L, Tonetti T, Quintel M. Regional physiology of ARDS. Crit Care. 2017; 21: 9–14. https://doi.org/10.1186/s13054-017-1905-9 PMID: 29297365

74. Al A, Aiad DA, Metwally AM, Rady AA. New mechanical ventilation strategies in acute respiratory distress syndrome. 2018; 1–6. https://doi.org/10.4103/1110-2098.234223

75. RC B. Insights Computed Tomography. Jama. 1993; 60612: 16–17.

76. Puybasset L, Cluzel P, Gusman P, Grenier P, Preteux F, Rouby JJ. Regional distribution of gas and tissue in acute respiratory distress syndrome. I. Consequences for lung morphology. Intensive Care Med. 2000; 26: 857–869. https://doi.org/10.1007/s001340051274 PMID: 10990099

77. Dakin O, Jones AT, Hansell DM, Hoffman EA, Evans TW. distribution in patients with ARDS. Respirology. 2012; 16: 1265–1272. https://doi.org/10.1111/j.1440-1843.2011.02048.x.Changes

78. Wolf SJ, Reske AP, Hammermüller S, Costa ELV, Spieth PM, Hepp P, et al. Correlation of lung collapse and gas exchange—A computer tomographic study in sheep and pigs with atelectasis in otherwise normal lungs. PLoS One. 2015; 10: 1–15. https://doi.org/10.1371/journal.pone.0135272 PMID: 26258686

79. Freitas ERFS De. Ventilação mecânica em pacientes com síndrome da angústia respiratória aguda Mechanical ventilation in patients with acute respiratory distress syndrome. 2007; 53–60.

80. Davison CA, Chapman SE, Sasser TA, Wathen C, Diener J, Schafer ZT, et al. Multimodal optical, X-ray CT, and SPECT imaging of a mouse model of breast cancer lung metastasis. Curr Mol Med. 2013; 13: 368–376. https://doi.org/10.2174/1566524011313030006 PMID: 23331009

81. Pelosi P, de Abreu MG. Acute respiratory distress syndrome: We can't miss regional lung perfusion! BMC Anesthesiol. 2015; 15: 14–16. https://doi.org/10.1186/s12871-015-0014-z PMID: 25792969